Surface supramolecular organization of a terbium (III) double-decker complex on graphite and its single molecule magnet behavior

Mathieu Gonidec,[†,‡] Roberto Biagi,[§,⊥] Valdis Corradini,[⊥] Fabrizio Moro,[§,] Valentina De Renzi,[§,⊥] Umberto del Pennino,[§,⊥] Domenico Summa,[≠] Luca Muccioli,[≠] Claudio Zannoni,[≠] David B. Amabilino,[,†] Jaume Veciana[*,†,‡]*

Institut de Ciència de Materials de Barcelona (ICMAB-CSIC), 08193 Bellaterra, Spain, Networking Center on Bioengineering, Biomaterials and Nanomedicine (CIBER-BBN), 08193 Bellaterra, Spain, Dipartimento di Fisica, Università di Modena e Reggio Emilia, Modena, Italy,

S3 Istituto Nanoscienze-CNR, Modena, Italy,

School of Chemistry, University of Nottingham, University Park, NG7 2RD Nottingham, United Kingdom, and Dipartimento di Chimica Fisica e Inorganica and INSTM, Università di Bologna, Viale Risorgimento 4, IT-40136 Bologna, Italy,

---

[†] ICMAB-CSIC

[‡] CIBER-BBN

[§] Università di Modena e Reggio Emilia

[⊥] Istituto Nanoscienze-CNR

[≠] Università di Bologna

Present address: University of Nottingham

E-mail: amabilino@icmab.es (D.B.A.) vecianaj@icmab.es (J.V.)

TITLE RUNNING HEAD: Terbium double-decker complex on HOPG as SMM

Abstract: The two dimensional self-assembly of a terbium (III) double-decker phthalocyanine on highly oriented pyrolitic graphite (HOPG) was studied by atomic force microscopy (AFM), and it was shown that it forms highly regular rectangular 2-D nanocrystals on the surface, that are aligned with the graphite symmetry axes, in which the molecules are organized in a rectangular lattice as shown by scanning tunneling microscopy (STM). Molecular Dynamics simulations were run in order to model the behavior of a collection of the double-decker complexes on HOPG. The results were in excellent agreement with the experiment, showing that – after diffusion on the graphite surface – the molecules self-assemble into nanoscopic islands which align preferentially along the three main graphite axes. These low dimension assemblies of independent magnetic centers are only one molecule thick (as shown by AFM) and are therefore very interesting nanoscopic magnetic objects, in which all of the molecules are in interaction with the graphite substrate and might therefore be affected by it. The magnetic properties of these self-assembled bar-shaped islands on HOPG were studied by X-ray magnetic circular dichroism (XMCD), confirming that the compounds maintain their properties as single-molecule magnets (SMM) when they are in close interaction with the metallic graphite surface.

Introduction

Single-molecule magnets (SMMs) are molecular compounds with a high spin ground state showing a slow magnetization relaxation rate at low temperatures.[1,2] Unlike bulk magnets, these superparamagnetic species do not present a permanent remnant magnetization, but some of them (like

the well known dodecamanganese clusters) have been shown to maintain a remnant magnetization over several months if kept at a sufficiently low temperature below their blocking temperature.[3] Since they typically present nanometric dimensions, they are potential candidates for high density data storage if properly organized on surfaces, with the ultimate goal of storing 1 bit per molecule.[4] Another possible application for such molecules could be in molecular spintronics.[5-7] Nevertheless, some issues needs to be addressed for them to be technologically exploitable, like their very low blocking temperature and the difficulties to organize and address individual molecules on surfaces.[8] While a lot of effort has been dedicated over the last few years to the preparation of new SMMs, trying to push-up their blocking temperatures (typically of the order of 5 K for the best compounds), very little has been done towards the addressing of an array of independent magnetic molecules. More importantly, a first step towards any technological application is to check that the properties of SMMs can be preserved when deposited on a surface, and that has been the subject of a very limited number of publications.[9-13]

Pc$_2$Tb
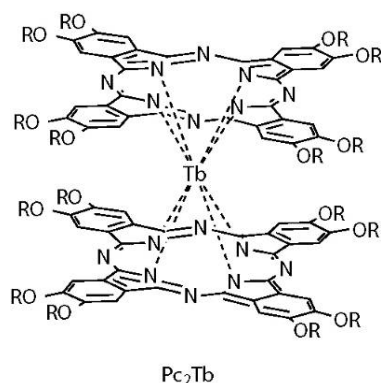
The double-decker phthalocyanine complexes of some lanthanide ions (Pc$_2$Ln), formed by the metal ion sandwiched between two phtalocyanine (Pc) dianionic ligands, have been shown recently to behave either in bulk, dilute solid solutions and even in frozen glass solution as single-molecule magnets.[14-17] On the other hand, some functionalized Pc$_2$Ln complexes were also shown to form well ordered self-assembled domains when deposited on highly oriented pyrolitic graphite (HOPG), although no information about the magnetic properties of such 2-D supramolecular organizations was available.[18,19]

As part of an ongoing program on multifunctional double decker complexes, we have focused on the preparation and characterization of 2-D arrays of double decker phthalocyanine complexes. Earlier

studies showed that complexes bearing peripheral butoxy substituents formed nicely ordered 2-D arrays on graphite but that the stability of those assemblies was limited to a few hours because the structured monolayers collapsed overnight.[18] For this reason we chose to prepare long alkoxy chain substituted complexes, in order to increase the number of van der Waals interactions with the substrate, so as to stabilize the monolayers. The known acetal protected complex $^iPc_2Tb$ (**1**)[20] was envisaged initially as a protected reaction intermediate towards a variety of alkoxy terminated phthalocyanines and accordingly it was prepared. However, during the course of this ongoing research program it was observed serendipitously that $^iPc_2Tb$ complex self-assembles as 2-D crystals on HOPG.

Here we present a detailed experimental and theoretical study of such 2-D supramolecular organizations on graphite as well as the magnetic behavior of such organizations characterized by X-ray magnetic circular dichroism (XMCD) comparing them with the bulk magnetic properties of this SMM.

Experimental Section

The starting materials were purchased from Sigma-Aldrich and used without any further purification. ^1H NMR spectra were recorded on a Bruker Avance DPX-360 spectrometer. The non deuterated solvent peak was used as an internal reference to calibrate the spectra ($CDCl_3$, 7.26 ppm). Mass spectra were recorded on a Bruker Ultraflex LDI-TOF spectrometer. UV-Vis absorption spectra were collected on a Varian Cary 5000 spectrometer.

Synthesis and Characterization.

4,5-Dibromocatechol (2). In a 500mL three neck round bottom flask under nitrogen, equipped with a reflux condenser, an addition funnel and a gas outlet connected to a bubbler filled with a 10% NaOH aqueous solution, was suspended catechol (136 mmol, 15.0 g, 1 eq.) in CCl_4 (150 mL). Bromine (272 mmol, 43.5 g, 2 eq.) diluted in CCl_4 (20mL) was added dropwise at 0 °C over 4.5 h. The excess of bromine was neutralized with aqueous $NaHSO_3$ (150 mL, 40% solution). The mixture was filtrated and the solids were dissolved in CCl_4, washed with water and dried in vacuum. The obtained 4,5-dibromocatechol (30.2 g) was then recrystallized from $CHCl_3$ (220 mL) to afford a white crystalline

solid (22.5 g, 84.0 mmol) with a yield of 62%. ^{1}H NMR (250 MHz, *CDCl$_3$*): δ 7.14 (s, 2 H, Ar-**H**), 5.43 (s, 2 H, -**OH**) ppm.

5,6-Dibromo-2,2-dimethyl-1,3-benzodioxole (3). To a suspension of 4,5-dibromocatechol (18.7 mmol, 5.0 g, 1.0 eq.) and acetone (1.644 ml, 22.4 mmol, 1.2 eq.), in dry toluene (30 ml) was added phosphorus trichloride (7.5 mmol, 0.65 ml, 0.4 eq.) dropwise at 20ºC over 30 minutes. The reaction was stirred over night at room temperature. Potassium carbonate (25 g) was added and the solids were filtered and washed with Toluene (50 mL). The organic layer was then washed with 10% NaOH (4x50 mL) dried on MgSO$_4$ and the volatiles were evaporated on a rotatory evaporator affording 5,6-dibromo-2,2-dimethyl-1,3-benzodioxole (2.4 g, 42%). FT-IR: 3110 (w), 3058 (w), 2991 (w), 2929 (w), 1697 (w), 1649 (w), 1600 (w), 1488 (s), 1459 (m), 1379 (s), 1362 (m), 1259 (m), 1239 (s), 1206 (m), 1078 (m), 980 (m), 914 (m), 855 (s), 827 (w), 782 (m), 693 (w), 659 (w), 595 (w), 516 (m) cm^{-1}. ^{1}H NMR (250 MHz, (CD$_3$)$_2$CO): 7.12 (s, 2H, Ar-**H**), 1.69 (s, 6H, -C(**CH$_3$**)$_2$) ppm.

4,5-Isopropylidenedioxyphthalonitrile (4). In a dry round-bottom flask under argon were suspended 5,6-dibromo-2,2-dimethyl-1,3-benzodioxole (9.99 mmol, 3.08 g, 1.0 eq.), tetrakis(triphenylphosphine) palladium(0) (0.99 mmol, 1.15 g, 0.1 eq.) and zinc cyanide (12.0 mmol, 1.41 g, 1.2 eq.) in DMF (20 mL). The mixture was then heated at 120 ºC for 2 h after which ammonia (37%, 100 mL) was added, and the resulting precipitate was filtrated, washed with more ammonia (100 mL) and purified by column chromatography of silicagel using toluene as an eluent, affording 4,5-isopropylidenedioxyphthalonitrile (1.7 g, 85%) as a white solid. FT-IR: 3123 (w), 3067 (w), 2995 (w), 2943 (w), 2229 (s), 1741 (w), 1651 (w), 1598 (m), 1546 (w), 1501 (s), 1452 (m), 1402 (w), 1381 (s), 1282 (s), 1264 (m), 1255 (m), 1210 (s), 1165 (m), 1119 (m), 982 (s), 879 (s), 873 (s), 826 (s), 775 (m), 731 (w), 654 (m), 534 (s), 513 (w) cm^{-1}. ^{1}H NMR (250 MHz, CDCl$_3$): 7.05 (s, 2H, Ar-**H**), 1.75 (s, 6H, -C(**CH$_3$**)$_2$) ppm.

Bis-(tetrakis-isopropylidenedioxy-phthalocyaninato) terbium (III) (^{i}Pc$_2$Tb; 1). In a flame dried Schlenk tube under argon was introduced 4,5-isopropylidenedioxyphthalonitrile (0.5 mmol, 100 mg, 1.0 eq.), and then the tube was degassed and purged with argon 3 times. Dry hexanol (1,5ml) was added with a syringe. DBU (0.25 mmol, 38 mg, 0.5 eq.) was added, and after stirring for 5min under argon,

Tb(OAc)$_3$.[H$_2$O]$_6$ (0.08 mmol, 35mg, 0.16 eq.) was added at once. The mixture was then warmed up in a sand bath to reflux at 160ºC for 16h. The course of the reaction was monitored by UV-Vis. After this time, the mixture was cooled to room temperature and acetonitrile was added to precipitate the complex. The dark green precipitate was filtered and dried in air. It was then purified by column chromatography with silicagel and by repeated size exclusion chromatography (on Biobeads SX1) using in both cases toluene as an eluent. The title compound was obtained (21 mg, 19%) as a dark green powder. MS m/z: 1759 (M$^+$). FT-IR: 2985 (w), 2921 (w), 2852 (w), 2782 (w), 1732 (w), 1599 (w), 1456 (s), 1387 (s), 1315 (m), 1270 (s), 1206 (s), 1125 (m), 1068 (s), 1010 (m), 976 (s), 860 (s), 837 (s), 752 (m), 723 (m), 680 (w) cm-1. UV-Vis (log(ε), toluene): 292 (4.90), 336 (4.90), 371 (5.03), 483 (4.52), 581 (4.17), 605 (4.40), 667 (5.13) nm.

Atomic force microscopy. The atomic force microscopy (AFM) images were recorded on a PicoSPM system (Molecular Imaging). The intermittent contact mode was used close to resonance frequencies of the silicon cantilevers (Nanosensors, FM type force constant 1.2-3.5 N/m and tip diameter 5 nm) of around 60–70 kHz. All the images were recorded under atmospheric conditions.

Scanning tunneling microscopy. The scanning tunneling microscopy (STM) images were recorded in ultra-high vacuum on a VT-SPM system (Omicron). Imaging conditions were a tunneling current of 50 pA and a bias voltage of -0.4 V.

Magnetometry. The magnetization measurements of bulk samples were done on a Quantum Design PPMS magnetometer equipped with a Vibrating Sample Magnetometer (VSM). The sample consisted of 9.17 mg of complex **1** introduced in a gelatin capsule.

Molecular Dynamics Simulations.

The neutral ^{i}Pc$_2$Tb complex was modeled with an atomistic force field (FF) in three separate units, a Tb^{4+} cation, and two ^{i}Pc^{2-} anions, without chemical bonds between them. The complex is then kept together, and also assembles spontaneously in the simulation, by the strong electrostatic interactions between the oppositely charged metal and ligands, and its geometry is determined by the balance of electrostatic interaction and steric repulsion, in analogy with lanthanide-water complexes.[21] The atomic

charges on $^iPc^{2-}$ atoms have been calculated at the optimized geometry with the B3LYP functional and 6-31G* basis set with the Gaussian09 software.[22] Also the parameters for the torsions involving nitrogen carbon atoms were calculated at this level for a negatively charged fragment of the ^iPc (see Supporting Information). The reason for this reparameterization is that, due to its quinoidal character, the charged Pc is more rigid than the neutral one and that general purpose FF parameters are typically derived for neutral molecules. The Lennard-Jones parameters for Tb^{4+} were set equal to the ones derived for Eu^{3+}/Gd^{3+} by van Veggel et $al.$[23] (σ=3.3 Å, ε=0.05 kcal/mol). A comparison of the energy-minimized geometry of the complex obtained by our force field with the crystal structure of a similar Tb-phthalocyanines complex present in the Cambridge Crystallographic database (JERGAP),[24] showed that the distances between Tb^{4+} and the $^iPc^{2-}$ nitrogens were well reproduced by the FF. All the other parameters for the $^iPc_2Tb$ complex were taken from the GAFF force field.[25]

Rectangular, defect-free graphite sheets with thickness of 4 atomic layers were built by replicating the crystalline cell of graphite of 60 x 40 x 2 times (hence four carbon sheets in the z direction). The interaction of graphite atoms with the complexes was parameterized with the Steele's potential,[26] using a cutoff of 18 Å. The electrostatic interactions, which act only between the complexes (in our model graphite atoms do not bear atomic charges), was calculated with the smooth particle mesh Ewald method, with mesh size of 1.2 Å. Different ways of modeling thermal exchange between the graphite surface and the complexes were tried, as described in Supporting Information section 4. The simple approach of keeping graphite atoms fixed resulted to be essentially equivalent in terms of structures obtained as the other more elaborate schemes involving surface atoms vibrations and will be adopted in what follows, except when stated otherwise.

All Molecular Dynamics (MD) simulations were run at constant volume and temperature (300 K) with the NAMD code[27] and 3D periodic boundary conditions; the graphite rectangle sides were oriented parallel to the x and y Cartesian axes and the z box side was set to 600 Å to mimic, in practice, a slab geometry with 2D periodic boundary conditions.

XMCD measurements.

The XMCD experiments were carried out at the ID8 beamline of the European Synchrotron Radiation Facility (ESRF) in Grenoble (France). The x-ray absorption spectra (XAS) were taken at the $M_{4,5}$ absorption edge of Tb in total electron yield mode using circularly polarized light with about 100% polarization degree. Temperature and external magnetic field were 7K and up to 5T, respectively. The measurements were done using an attenuated beam flux in order to avoid radiation exposure induced sample degradation. Integrity checks based on XAS spectra were performed throughout the experiment, never finding any trace of degradation. The direction of the impinging beam was parallel to the applied magnetic field (H) and both were perpendicular to the sample surface. The dichroic spectrum was obtained as the difference between the absorption spectra taken with the helicity of the incident photon antiparallel ($I^{\uparrow\downarrow}$) and parallel ($I^{\uparrow\uparrow}$) to the applied magnetic field (H). This spectrum is then normalized to the maximum intensity of the unpolarized spectrum ½($I^{\uparrow\downarrow}$ + $I^{\uparrow\uparrow}$). In the hypothesis that the XMCD spectrum holds its shape, its intensity is proportional to the projection of the magnetic moment of the absorbing atom on the direction of the photon wave vector,[28] therefore the hysteresis curves can be obtained by recording the XMCD signal as a function of the applied magnetic field.

Results and Discussion

Synthesis. The isopropylidene-dioxy substituted double-decker terbium complex **1** ($^{i}Pc_2Tb$) was prepared in three steps from 4,5-dibromocatechol (**2**) with small changes from an established method.[20]

Compound **3** was prepared from a solution of **2** in toluene with a stoichiometric amount of acetone by the dropwise addition of a solution of PCl_3 in toluene. The corresponding phthalonitrile **4** was prepared in high yield by a tandem zinc-palladium catalyzed cyanation of **3**, instead of employing the classical Rosenmund-von Braun conditions. Indeed, the tandem zinc-palladium method allows the formation of phthalonitriles from 1,2-dibromoaryl derivatives at 120ºC only and with almost stoichiometric amount of zinc cyanide.[29]
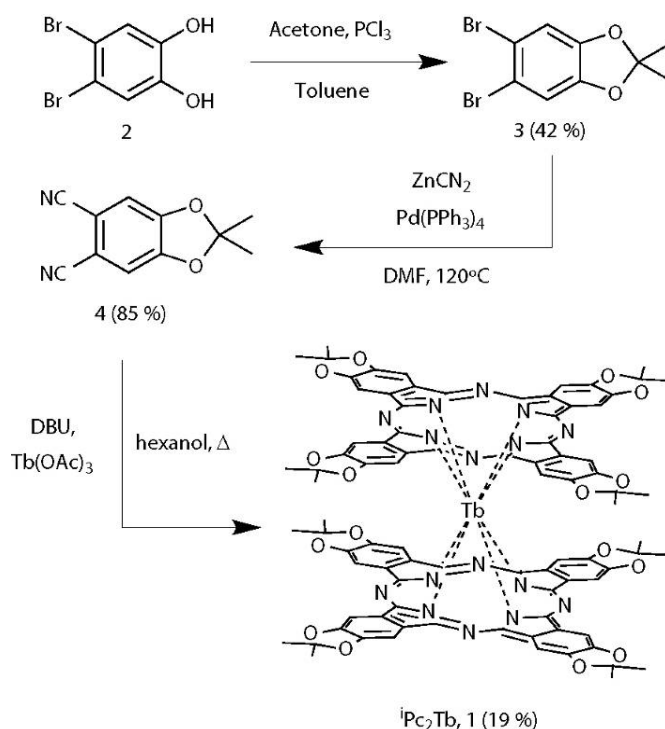
Scheme 1. Synthesis of ^{i}Pc$_2$Tb (**1**) in three steps from 4,5-dibromocatechol (**2**) using a one-step methodology from the corresponding phthalonitrile **4**.

These more gentle conditions, as compared to the Rosenmund von Braun reaction which requires temperatures of around 150ºC and great excess of cyanide, allow preparation of the target phthalonitriles in higher yield, avoiding for instance the formation of copper phthalocyanine as an undesired by-product. Finally, the double-decker terbium complex **1** was achieved by reacting compound **4** with terbium (III) acetate in the presence of DBU in refluxing n-hexanol. Complex **1** was obtained as a dark green powder which is stable at ambient conditions.

Surface deposition. In order to investigate the self-assembly properties of complex **1**, dilute solutions of the double-decker terbium complex in toluene were prepared. These solutions were dropcast onto freshly cleaved HOPG under ambient conditions. The solvent was allowed to evaporate and the obtained monolayers were studied, directly after deposition, by atomic force microscopy (AFM) in acoustic mode. The optimal deposition condition corresponded to a 10^{-6}M solution of **1**. Thus, after warming up such a solution with a heat gun, it was dropcast onto freshly cleaved HOPG and covered with a Petri dish in order to obtain a slow and regular evaporation of the solvent, allowing therefore

approach the supersaturation slowly. In these conditions, compound **1** formed highly regular anisotropic bar-shaped islands of a few hundreds of nanometers long by approximately fifty nanometers wide (see Figure 1). It is also worth stressing that these bar-shaped islands are not randomly distributed on the graphite surface. Indeed they are disposed in such a way that they form angles of about 120º amongst themselves which is a strong indication that the growth of these supramolecular organizations happens along one of the three main graphite symmetry directions. The anisotropy of these bars can be explained by a difference in the kinetics of crystallization along and across the graphite main axes. Namely, the crystallization rate is higher along one of the substrate's axes while the lateral growth seems to be less favored. The height or thickness of the self-assembled nanoislands was of approximately 1.1-1.3 nm as shown in Figure 1C and 1D. The tops of the bar-shaped islands are relatively smooth, indicating a high degree of structural order, as is expected for a crystalline material.
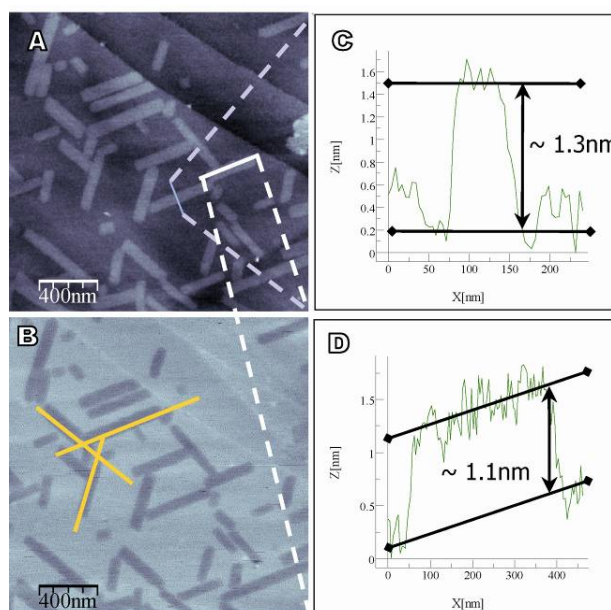
Figure 1. (A) Topography and (B) phase AFM images of the self-assembled bar-shaped islands formed by complex **1** on HOPG as dropcast from a 10^{-6}M solution in toluene. In (B) in yellow are depicted the three different orientations of the bars. In (C) and (D two profiles showing the thickness of the bars in part (A) are shown.

Ideally, the expected height of a monolayer of molecules of complex $^{i}Pc_2Tb$, when arranged flat on graphite, can be estimated by summing the interplanar distance of the two phthalocyanine rings, plus two times the distance of the outer hydrogen atoms from the plane of the phthalocyanine ligands, and two times the van der Waals radius of hydrogen (see Figure 2). The interplanar distance of the complex was estimated to be of 3.9-4.0 Å from the X-ray structure of another neutral double-decker phthalocyanine complex.[30] The distance of the outer hydrogen atom from the plane of the phthalocyanines was estimated to be of approximately 2.0 Å from the crystal structures of other benzodioxole compounds[31] and confirmed by PM3 molecular mechanics on 2,2-dimethyl-benzo dioxolane. Finally, a value of 1.1 Å was used as the van der Waals radius of hydrogen.[32] The total estimated height of the monolayers on graphite is then 10.1-10.2 Å, i.e. 1.0 nm. On the other hand, the diameter of the complex was estimated to be of approximately 22.8 Å or 2.3 nm, i.e. 20.6 Å plus two times the van der Waals radius of hydrogen. All these estimated dimensions suggest therefore strongly that the double-decker molecules should lay flat on the surface and the bar-shaped nanoislands are one molecule thick.
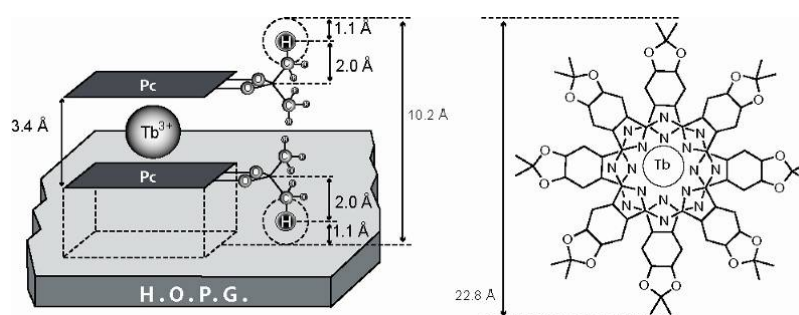
Figure 2. Schematic representation of complex $^{i}Pc_2Tb$ on top of the graphite (left) and lateral dimensions of the complex (right).

The morphology of bar-shaped nanoislands could be seen over large areas of the sample, in different locations of the graphite and on different samples. The size distribution of the nanoislands on the graphite was estimated by measuring 170 different bar-shaped islands. The width of the nanocrystals was thus estimated to be of $w = 70 \pm 30$ nm, and their length $l = 250 \pm 150$ nm indicating that they

correspond to 2D crystals of approximately $1 \times (30 \pm 13) \times (108 \pm 65)$ molecules; i.e. this is c.a. 5300±2000 molecules. This value agrees with that of ~5000 molecules calculated from the simulation using the surface area per molecule obtained for the supramolecular aggregates by Molecular Dynamics (*vide infra*).

In order to get more insight into the internal organization of the nanoislands, a dropcast sample prepared from a 10^{-6}M solution of **1** in toluene – employing the same deposition conditions as those used for the AFM experiment – was studied by scanning tunneling microscopy (STM). Complex **1** was shown to form packed layers composed of ordered rows of molecules (see Figure 3).
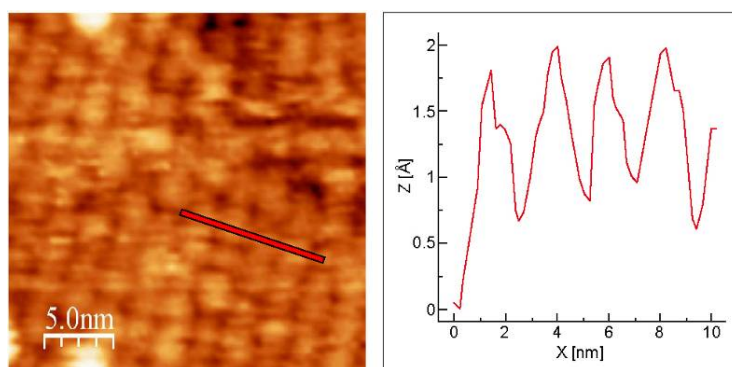
Figure 3. (left) STM image of the self-assembled layer formed by complex **1** on HOPG as dropcast from a 10^{-6}M solution in toluene. (right) depth profile measured across four rows of molecules. The distance from one row to the other is of approximately 2.1-2.3 nm.

The structure of the layer was found to be rectangular. Interestingly, the distance between adjacent rows of molecules was found to be of approximately 2.1-2.3 nm which is in good agreement with the estimated lateral dimensions of complex **1** (see Figure 2).

Molecular Dynamics Simulations. In order to confirm and enrich the experimental observations, a few room temperature studies were performed with the MD technique, differing among them on the number of complexes and on the dimension of the graphite surface, but always at low coverage, sub-monolayer conditions. In all of them, the $^{i}Pc_2Tb$ complexes exhibited the tendency to lay flat ("face-

on") on the surface, maximizing the van der Waals interaction with the graphite, and not to stack one onto each other to form π-aggregates.

In analogy with similar terbium(III) double-decker phtalocyanine complexes,[12] the adopted force field predicts that in each complex the two phthalocyaninates groups are eclipsed with an angle varying from 30 to 45 degrees, probably both for minimizing the steric repulsion between the methyl groups and the electrostatic repulsion between equivalent atoms (thus bearing the same atomic charge) on the two moieties. In addition this conformation allows some interaction between the arms of the uppermost $^{i}Pc^{2-}$ and the substrate. Isolated and aggregated complexes show also a preferential orientation of the $^{i}Pc^{2-}$ arms with respect to one of three equivalent graphite axes: typically, one of the two arms of the lowermost $^{i}Pc^{2-}$ is on average parallel to one of the axes, with angular displacements of about 10 degrees (see Figure 4). As a matter of fact, this orientation maximizes the π-π interaction with graphite, while the reason for the small angular displacement is again the steric encumbrance of the methyl groups jutting out of the phthalocyanine plane.
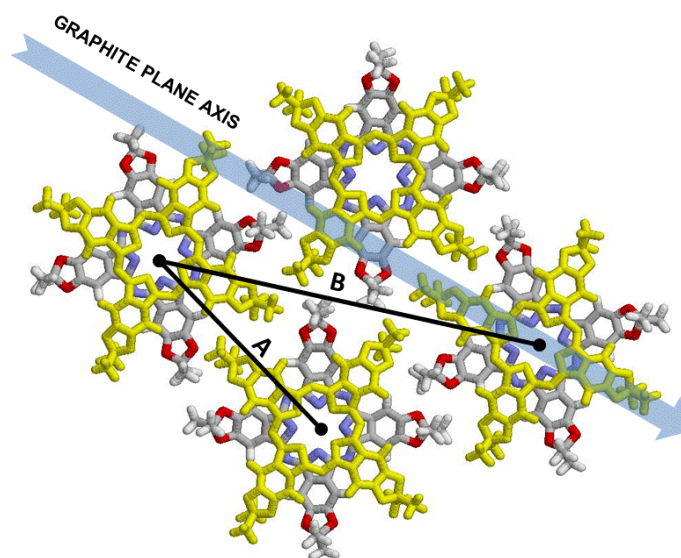
Figure 4. Scheme of the two dimensional aggregation of $^{i}Pc_2Tb$ complexes on HOPG obtained from MD simulations (Terbium ions are not shown). The $^{i}Pc^{2-}$ lying directly on graphite (depicted in yellow), have one of their arms on average parallel to the graphite axis, and this direction correspond to the favorite direction of growth of the aggregate. The uppermost $^{i}Pc^{2-}$ (CPK colored) are twisted of about 45

degrees with respect to the growth direction. These 2D crystals present an approximately hexagonal lattice with side A=19.5±1 Å (B=33±2 Å).

To probe the self-assembling behavior we studied the evolution of the position of 24 complexes from a starting configuration in which they were placed, to maximize the distance among them, on a regular lattice on the 60 x 40 x 2 graphite slab (Figure 5a). Immediately the SMM started to diffuse on the surface until forming several small aggregates, still able of translating, which finally coalesced in a single nanocrystal after about 10 ns (see Figure 5b and movie at Supporting Information). The same dynamic behavior and the shape of the final aggregate was previously verified in other simulations of smaller or similar size (see also Figure S3 at ESI), hence we are confident of its reproducibility.

Figure 5. (a) Initial placement of complexes before the MD aggregation simulation. (b) 2D nanocrystals formed by 24 molecules after 10 ns , (c) Calculated topography map of (b), showing that the maximum height of the 2D aggregate is about 1 nm.

Despite the sample being relatively large for the MD standards (40392 atoms), the aggregate is constituted of only 24 complexes and its dimensions are then very small in comparison with the real aggregates shown in Figure 2; its limited size and the presence of several defects (cf. Figure 5A) prevent the exact calculation of crystalline cell and lattice parameters. However, the comparison with the experimental results is rewarding and can indeed be attempted. Besides the spontaneous aggregation process, it is interesting to note that the tendency to grow along directions parallel to the graphite axes is confirmed by the shape of the simulated nanocrystal. The three graphite axes form an angle of 120

degrees among each other, and this is matched in the aggregate through the onset of an apparently hexagonal lattice (scheme in Figure 4). Phthalocyanines are known to form either hexagonal or rectangular lattices or both;[33] in this case we cannot distinguish between the two, but only estimate the distances between the first and second neighbors in the crystal (A=19.5±1 and B=33±2 Å). These values, assigned by inspecting the radial distribution of Tb atoms (Figure S2 at ESI), are compatible within the error bars with both rectangular and hexagonal lattices, both possibilities being in good agreement with the morphology experimentally observed by STM. Interestingly, the lattice size is slightly shorter than the length of the Pc arm (estimated to be 22.8 Å), and this is accomplished through the in-plane interdigitation of the acetal groups, for a presumed total area per molecule of 342±30 Å^2. Again, the lattice size is in good agreement with the row to row distance measured by STM (see Figure 3). For what regards the height of the aggregate, the calculated topography map in Figure 5B is again in agreement with the experimental results of Figure 1, showing maximum heights of the order of 10 Å (1 nm) in correspondence of the acetal methyl groups. In a last series of calculations we investigated the origin of the growth of the crystals along the graphite axis. To this end we estimated the energy landscape for positioning a new complex close to an aggregate of eight molecules aligned with a graphite axis; the obtained energy map (Figure S2 at ESI) indicates that there are no preferable growth directions from an energetic point of view, i.e. the energy gain for adding a ^{i}Pc$_2$Tb to a formed 2D crystal (approximately 10 kcal/mol) does not depend on the orientation and the position of the complex with respect to the nanocrystal axes. To evaluate also the kinetic effects, we ran a simulation of a single complex on graphite at 500 K and studied its diffusion on the surface as function of the orientation with respect to the graphite axes. It turned out that diffusion is indeed faster along these three directions; these results let us suppose that the shape of the 2D crystals is templated by graphite through kinetic, more than energetic effects.

Magnetic behavior. The well defined morphology of the sub-monolayers of complex ^{i}Pc$_2$Tb, is a good example of a low dimensional assembly of independent SMMs. For this reason, the magnetic behavior of these 2D crystals resulted very interesting from the magnetic point of view. It is worth

mentioning that all molecules of complex $^iPc_2Tb$ lay directly on the surface graphite and therefore all of them could be affected by it in some way. It is of great importance to know whether they retain their SMM behavior under such conditions.

Before doing such a study we characterized the dynamic magnetic behavior of a bulk sample of complex $^iPc_2Tb$ by ac-magnetic susceptometry (see Figure 6).
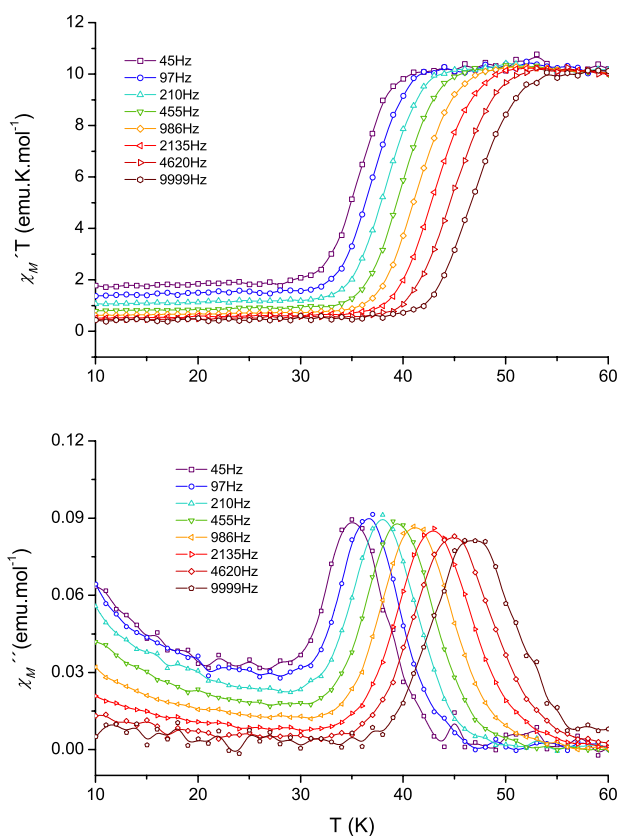
Figure 6. Temperature and frequency dependence of the in-phase (above) and out of phase (below) ac magnetic susceptibility of a microcrystalline bulk sample of **1**.

The blocking temperature of complex $^iPc_2Tb$ in solid state at 986 Hz was found to be 41 K which is significantly smaller than the literature value (49 K) for the unsubstituted neutral double-decker terbium complex Pc_2Tb **5** at almost the same frequency (997 Hz) and under the same conditions.[34] Indeed it means that the relaxation time of $^iPc_2Tb$ at 49 K is of approximately 3.4×10^{-5} s, thirty times smaller than the literature value of 1×10^{-3} s for Pc_2Tb. The Arrhenius analysis (see Figure 7) showed that the magnetic relaxation of compound $^iPc_2Tb$ in a bulk sample follows a thermally activated process with a

pre-exponential factor of $\tau_0^{-1} = 2.61 \times 10^{11}$ s^{-1} and an effective barrier height of $\Delta = 556$ cm^{-1}. This process could be fitted by a Debye function with dispersion parameter $\alpha = 0.11$, as a Cole-Cole plot (see ESI).
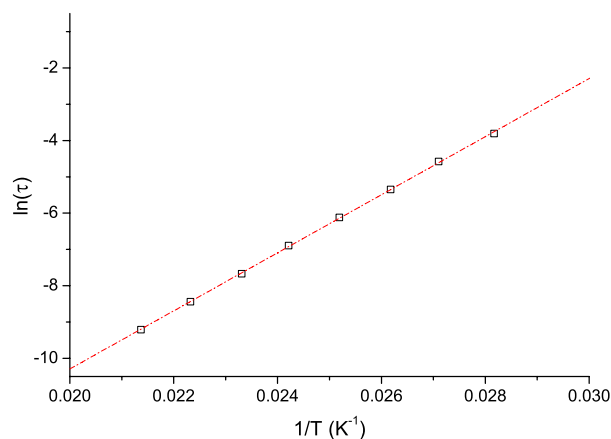
Figure 7. Arrhenius plot of the natural logarithm of the relaxation time τ of complex **1**.

The values obtained from the Arrhenius analysis are both significantly higher than those found for a powder sample of the unsubstituted neutral Pc$_2$Tb complex, 6.8×10^8 s^{-1} and 410 cm^{-1}, respectively, explaining the apparent different relaxation rates exhibited by both SMMs. The hysteresis of magnetization of a bulk sample of complex ^{i}Pc$_2$Tb was first recorded at 7 K as a control experiment.
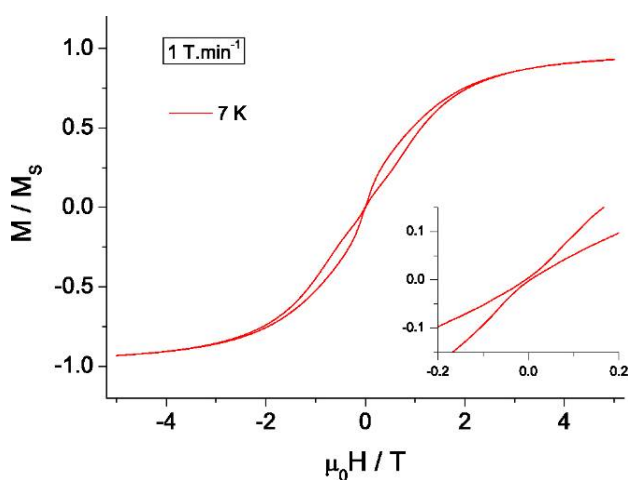
Figure 8. Bulk magnetization hysteresis of an amorphous bulk sample of **1** measured at 7 K. *Inset*: Zooming of the region at low magnetic fields.

The obtained magnetization hysteresis curve is shown in Figure 8. A butterfly-shaped hysteresis,[35] typical in these complexes,[15] was observed. Thus, the magnetization collapses at $\mu_0H = 0$ T where almost no coercive field can be observed.

In order to characterize the magnetic response of molecules of complex $^iPc_2Tb$ deposited on a HOPG surface, two samples were prepared: a submonolayer sample, named as $^{ML}1$, prepared in the dropcasting conditions described earlier, and a thick layer sample $^{TL}1$, prepared by repeating ten times the previous dropcasting procedure with a more concentrated $(10^{-3}M)$ solution of **1**.

The differences between samples $^{ML}1$ and $^{TL}1$ should indicate the influence of the surface on the magnetic behavior of the molecules. Indeed, while the submonolayer $^{ML}1$ must be strongly influenced by the interaction of all the molecules of the nanoislands with the surface, the thick layer should behave essentially like the bulk compound in which the majority of molecules only feel the neighboring analogous molecules.

The two samples were studied by X-ray magnetic circular dichroism (XMCD) spectroscopy.[36] In this technique, two circularly polarized X-ray absorption spectra (XAS) of complex **1** are measured at the $M_{4,5}$ edge of Tb^{3+} ion with the helicity of the incident radiation parallel and antiparallel to the applied magnetic field, respectively. The difference between these two spectra, normalized to the maximum intensity of the unpolarized spectrum, provides the XMCD spectrum (see Figure 9). The incident X-ray photon excites a 3d core electron to the 4f level and therefore it gives information on the 4f electronic structure governing the magnetic behavior of the terbium ion. The direction of the impinging beam was parallel to the applied magnetic field (H) and both were perpendicular to the sample surface. If the XMCD spectrum holds its shape, its intensity is proportional to the projection of the magnetic moment of the absorbing atom on the direction of the photon wave vector and,[28] therefore the hysteresis curves can be obtained by recording the XMCD spectrum as a function of the applied magnetic field. The acquisition of the full spectra, however, is time consuming. A way to speed-up the measurements was the acquisition of the maximum value of the XMCD spectrum by recording the XAS intensity at only two points for each magnetic field value, instead of acquiring the full XAS spectrum, namely at a pre-

edge point (1225 eV) and at the energy corresponding to the maximum value of the XMCD signal (1237.6 eV). This is done cycling twice the magnetic field, one cycle for each photon polarization. The intensity values were registered while maintaining the field constant. We adopted this procedure after having checked that the shape of the XMCD spectrum remains the same while varying the magnetic field. A detailed study of the XMCD spectrum of **1** is described elsewhere.[37] In that work, in particular, we proved that the maximum value of the Tb dichroic spectrum is actually proportional to the total Tb magnetization. The hysteresis of XMCD signal were then obtained at an average speed of 1.0 T.min^{-1}.

The obtained XMCD detected magnetization curves, recorded for $|\mu_0H| \leq 5T$ as described above, are shown in Figure 10.
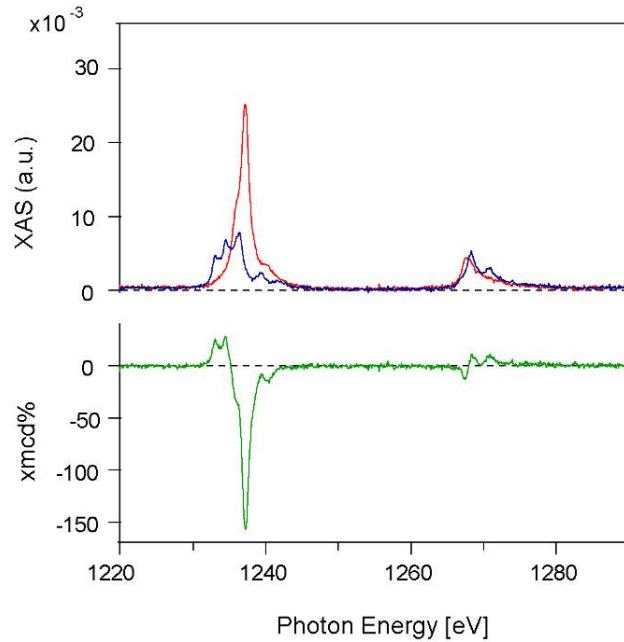
Figure 9. XAS spectra at the $M_{4,5}$ edge of Tb for ^{ML}**1** with helicities parallel ($I^{\uparrow\uparrow}$, in red) and antiparallel ($I^{\uparrow\downarrow}$, in blue) to an applied magnetic field of 5 T at 7 K (above) and the XMCD spectrum given by their difference normalized to the maximum intensity of the unpolarized spectrum ½($I^{\uparrow\downarrow}$ + $I^{\uparrow\uparrow}$) (below in green).[37]

At first glance, the hysteresis curves of ^{ML}**1** and ^{TL}**1** samples look quite similar in shape. However, it is worth noting that the butterfly loops are more open for the thick film ^{TL}**1** as for the submonolayer sample ^{ML}**1**. There is almost no remnant magnetization for either of the two samples in these conditions,

and the coercive field of the submonolayer sample (see inset in Figure 10) is not significantly different from zero, which is to be expected at this temperature (see the 7 K bulk measurement inset in Figure 8).

While they differ slightly from one another, ^{ML}1 and ^{TL}1 are both very similar to the bulk measurement made in the same conditions (7 K), which means that the magnetic behavior of **1** is essentially preserved when deposited on the graphite surface. As it appears, there is therefore not much influence of the surface on the magnetic properties of complex **1**, being the interaction between the surface and molecules not able to annihilate the SMM behavior.
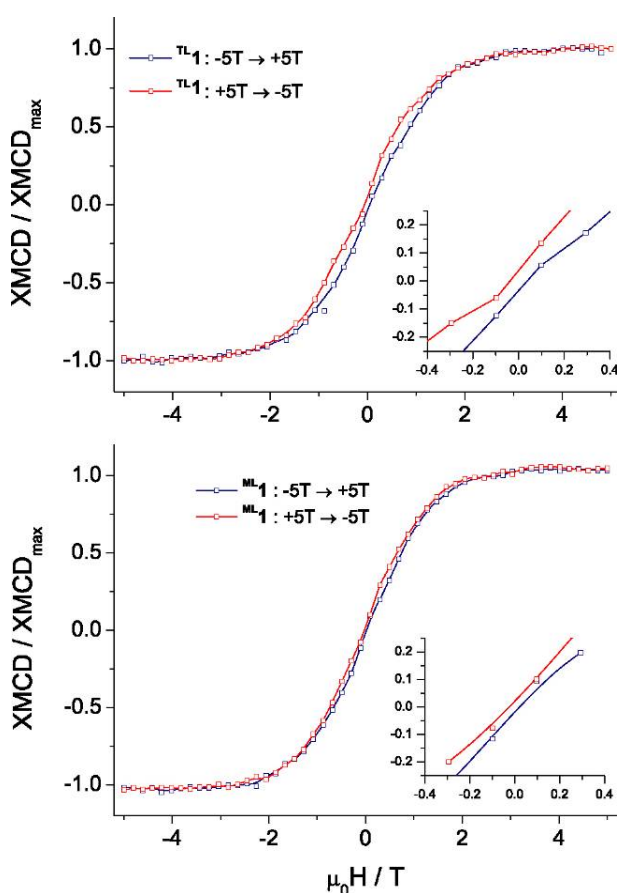
Figure 10. XMCD detected hysteresis of magnetization for the thick layer sample ^{TL}1 (above) and the monolayer sample ^{ML}1 (below) on HOPG measured at 7 K (see text). The inset shows the enlargement of the central part of both hystereses.

Conclusions

20

The double-decker phthalocyanine lanthanide complex [i]Pc$_2$Tb self-assembled on HOPG forms highly regular rectangular 2-D nanocrystals that are aligned with the three main graphite axes. XMCD was used as a successful tool to record the magnetization hysteresis of the complex [i]Pc$_2$Tb adsorbed onto the graphite surface.

Unlike the previously described Fe$_4$ on gold,[38] it is important to notice that here the terbium complexes are not wired covalently to the surface by a long alkyl chain but are on the contrary lying directly on top of the graphite surface. In principle, the perturbation induced by the surface on [i]Pc$_2$Tb could have destroyed the SMM properties, but the XMCD magnetization hysteresis measurements showed that this is not the case, and therefore that this assembly procedure is an interesting one for the preparation of SMM arrays.

Two very recent contributions present the magnetic behavior of non-substituted double-decker complexes on Au(111) and Cu(100),[9,13] showing that TbPc$_2$ does not present any hysteresis of magnetization when deposited on Cu(100), while on Au(111) it is clearly observed. It is worth noting the presence of an open butterfly hysteresis both in thick and thin layers of TbPc$_2$ on Au(111). The latter shows a narrower hysteresis than the former one; a result which is consistent with those presented here.

To the best of our knowledge, it is the first time that magnetization hysteresis is observed for molecules of a double-decker phthalocyanine lanthanide complex that are all in intimate contact with a graphite surface. Importantly, the slow magnetic relaxation rate, characteristic of these compounds is still present in a well-characterized submonolayer sample of the neutral [i]Pc$_2$Tb complex and the behavior of the sample is not very different from the bulk complex measured in the same conditions.

Spain. D.S, L.M. and C.Z. acknowledge Stefano Zacchini (University of Bologna) for useful suggestions. We warmly thank Amable Bernabé (ICMAB-CSIC) for recording IR and LDI-TOF spectra. We acknowledge the ESRF for provision of beamtime and we are grateful to J.C. Cezar (ESRF) for his precious assistance in using beamline ID8.

Supporting information. The following information is included: 1) Complete reference #20; 2) Calculation of the potential for torsions involving aromatic nitrogens in phthalocyaninates; 3) Movie of the Molecular Dynamics aggregation experiment; 4) In plane radial distribution of aggregates; 5) Potential energy map for adding a new complex to an aggregate of 8 ^{i}Pc$_2$Tb; 6) Measurement of the diffusion of a single complex on graphite; 7) Cole-Cole plot at 40 K for a microcrystalline sample of ^{i}Pc$_2$Tb. This material is available free of charge via the Internet at http://pubs.acs.org.

References

(1)   Gatteschi, D.; Sessoli, R.; Villain, J. *Molecular Nanomagnets*; Oxford University Press: Oxford, 2006.

(2)   Gatteschi, D.; Bogani, L.; Cornia, A.; Mannini, M.; Sorace, L.; Sessoli, R. *Solid State Sci.* **2008**, *10*, 1701.

(3)   Gatteschi, D.; Sessoli, R. *Angew. Chem. Int. Ed.* **2003**, *42*, 268.

(4)   Cavallini, M.; Gomez-Segura, J.; Ruiz-Molina, D.; Massi, M.; Albonetti, C.; Rovira, C.; Veciana, J.; Biscarini, F. *Angew. Chem. Int. Ed.* **2005**, *44*, 888.

(5)   Affronte, M. *J. Mater. Chem.* **2009**, *19*, 1731.

(6)   Rocha, A. R.; Garcia-suárez, V. M.; Bailey, S. W.; Lambert, C. J.; Ferrer, J.; Sanvito, S. *Nat. Mater.* **2005**, *4*, 335.

(7)   Bogani, L.; Wernsdorfer, W. *Nat. Mater.* **2008**, *7*, 179.

(8)   Gatteschi, D.; Cornia, A.; Mannini, M.; Sessoli, R. *Inorg. Chem.* **2009**, *48*, 3408.

(9)   Margheriti, L.; Chiappe, D.; Mannini, M.; Car, P.; Sainctavit, P.; Arrio, M. A.; de Mongeot, F. B.; Cezar, J. C.; Piras, F. M.; Magnani, A.; Otero, E.; Caneschi, A.; Sessoli, R. *Adv. Mater.* **2010**, *22*, 5488.

(10)   Katoh, K.; Komeda, T.; Yamashita, M. *Dalton Trans.* **2010**, *39*, 4708.

(11)   Mannini, M.; Pineider, F.; Sainctavit, P.; Danieli, C.; Otero, E.; Sciancalepore, C.; Talarico, A. M.; Arrio, M.-A.; Cornia, A.; Gatteschi, D.; Sessoli, R. *Nat. Mater.* **2009**, *8*, 194.

(12)   Vitali, L.; Fabris, S.; Conte, A. M.; Brink, S.; Ruben, M.; Baroni, S.; Kern, K. *Nano Lett.* **2008**, *8*, 3364.

(13)   Stepanow, S.; Honolka, J.; Gambardella, P.; Vitali, L.; Abdurakhmanova, N.; Tseng, T.-C.; Rauschenbach, S.; Tait, S. L.; Sessi, V.; Klyatskaya, S.; Ruben, M.; Kern, K. *J. Am. Chem. Soc.* **2010**, *132*, 11900.

(14)   Ishikawa, N.; Sugita, M.; Ishikawa, T.; Koshihara, S.-y.; Kaizu, Y. *J. Phys. Chem. B* **2004**, *108*, 11265.

(15)   Ishikawa, N.; Sugita, M.; Wernsdorfer, W. *Angew. Chem. Int. Ed.* **2005**, *44*, 2931.

(16)   Ishikawa, N. *Polyhedron* **2007**, *26*, 2147.

(17)   Gonidec, M.; Davies, E. S.; McMaster, J.; Amabilino, D. B.; Veciana, J. *J. Am. Chem. Soc.* **2010**, *132*, 1756.

(18)   Gomez-Segura, J.; Diez-Perez, I.; Ishikawa, N.; Nakano, M.; Veciana, J.; Ruiz-Molina, D. *Chem. Commun.* **2006**, 2866.

(19)   Klymchenko, A. S.; Sleven, J.; Binnemans, K.; De Feyter, S. *Langmuir* **2006**, *22*, 723.

(20)   Ivanov, A. V.; Svinareva, P. A.; Zhukov, I. V.; Tomilova, L. G.; Zefirov, N. S. *Russ. Chem. Bull. Int. Ed.* **2006**, *55*, 281.

(21)   Kowall, T.; Foglia, F.; Helm, L.; Merbach, A. E. *J. Phys. Chem.* **1995**, *99*, 13078.

(22)   Frisch, M. J. *Gaussian 09, Revision A.1*; Gaussian, Inc.: Wallingford CT, 2009.

(23)   van Veggel, F. C. J. M.; Reinhoudt, D. N. *Chemistry – A European Journal* **1999**, *5*, 90.

(24)   Loosli, C.; Liu, S. X.; Neels, A.; Labat, G.; Decurtins, S. *Zeitschrift fur Kristallographie - New Crystal Structures* **2006**, *221*, 135.

(25)   Wang, J.; Wolf, R. M.; Caldwell, J. W.; Kollman, P. A.; Case, D. A. *J. Comput. Chem.* **2004**, *25*, 1157.

(26)   Steele, W. A. *J. Phys. Chem.* **1978**, *82*, 817.

(27)   Phillips, J. C.; Braun, R.; Wang, W.; Gumbart, J.; Tajkhorshid, E.; Villa, E.; Chipot, C.; Skeel, R. D.; Kalé, L.; Schulten, K. *J. Comput. Chem.* **2005**, *26*, 1781.

(28)   Chen, C. T.; Idzerda, Y. U.; Lin, H.; Meigs, G.; Chaiken, A.; Prinz, G. A.; Ho, G. H. *Phys Rev B Condens Matter* **1993**, *48*, 642.

(29)   Barrett, A. G. M.; Hanson, G. R.; White, A. J. P.; Williams, D. J.; Micallef, A. S. *Tetrahedron* **2007**, *63*, 5244.

(30)   Gurek, A. G.; Basova, T.; Luneau, D.; Lebrun, C.; Koltsov, E.; Hassan, A. K.; Ahsen, V. *Inorg. Chem.* **2006**, *45*, 1667.

(31)   Sun, D.; Rosokha, S. V.; Kochi, J. K. *J. Phys. Chem. B* **2007**, *111*, 6655.

(32)   Rowland, R. S.; Taylor, R. *J. Phys. Chem.* **1996**, *100*, 7384.

(33)   Olivier, Y.; Muccioli, L.; Lemaur, V.; Geerts, Y. H.; Zannoni, C.; Cornil, J. *J. Phys. Chem. B* **2009**, *113*, 14102.

(34)   Ishikawa, N.; Sugita, M.; Tanaka, N.; Ishikawa, T.; Koshihara, S.-y.; Kaizu, Y. *Inorg. Chem.* **2004**, *43*, 5498.

(35)   Chiorescu, I.; Wernsdorfer, W.; Müller, A.; Bögge, H.; Barbara, B. *Phys. Rev. Lett.* **2000**, *84*, 3454.

(36)   Funk, T.; Deb, A.; George, S. J.; Wang, H.; Cramer, S. P. *Coord. Chem. Rev.* **2005**, *249*, 3.

(37)   Biagi, R.; Fernandez-Rodriguez, J.; Gonidec, M.; Mirone, A.; Corradini, V.; Moro, F.; De Renzi, V.; del Pennino, U.; Cezar, J. C.; Amabilino, D. B.; Veciana, J. *Phys. Rev. B* **2010**, *82*, 224406.

(38)   Mannini, M.; Pineider, F.; Sainctavit, P.; Danieli, C.; Otero, E.; Sciancalepore, C.; Talarico, A. M.; Arrio, M. A.; Cornia, A.; Gatteschi, D.; Sessoli, R. *Nat. Mater.* **2009**, *8*, 194.